Intermetallics 182 (2025) 108762

Contents lists available at ScienceDirect

Intermetallics

journal homepage: www.elsevier.com/locate/intermet

Designing B2-phase ordered Cu-Pd-Ag-Ru microfiber with strength-conductivity combination via melt-extraction and isothermal annealing

Y.Y. Sun [a,b,1], Y.H. Gao [b,1], Y.B. Wang [b], Y. Huang [b], M.C. Jian [b], F.C. Wang [b], Y. Li [b], L. Fu [b], X. Jin [b], H.B.C. Yin [b], J. Xu [b], S.D. Feng [c], J.Q. Wang [b,*], J.T. Huo [b,**], M. Gao [b,***]

[a] School of Materials Science and Chemical Engineering, Ningbo University, Ningbo, 315211, China
[b] Ningbo Institute of Materials Technology and Engineering, Chinese Academy of Sciences, Ningbo, 315201, China
[c] Center for Advanced Structural Materials, State Key Laboratory of Metastable Materials Science and Technology, Yanshan University, Qinhuangdao, Hebei, 066004, China

ARTICLE INFO

Keywords:
Copper alloy
Microfiber
Strength
Electrical conductivity
B2 phase
Nano-precipitate

ABSTRACT

Copper alloys are widely used in the electrical and electronic devices due to their excellent electrical and thermal conductivity. However, the trade-off relationship between strength and conductivity limits their application in the electrical contacts and circuit leads. In this study, an experimental strategy based on melt extraction and appropriate post-heat treatment was proposed to design one kind of B2-phase ordered Cu-Pd-Ag-Ru microfiber. It was found that this microfiber displays the excellent comprehensive performance of the strength and the conductivity. In comparison with the cast alloy, the strength for the designed microfiber is increased by 2.75 times and there appears the 70 % enhancement for the electrical conductivity. The strengthening mechanisms can be attributed to the phase transition from FCC to B2 phase, grain refinement, and the formation of Ru and Ag precipitates. Furthermore, the significant improvement in electrical conductivity is primarily due to the introduction of the B2 ordered phase and the elongation of longitudinal grains. The current study not only provides one kind of excellent copper alloys for the electrical contacts and circuit leads, but also offers a new strategy for surmounting the strength-conductivity trade-off in metals.

1. Introduction

Conductor materials are of vital importance in a wide range of applications including rail transportation, military, aviation, electronics and numerous other fields, as high electrical conductivity and high strength are indispensable in these areas. Copper and its alloys are extensively utilized in the electronic industry, high energy facilities, rail transportation and other fields because of their remarkable electrical conductivity, thermal conductivity, corrosion resistance, easy-to-process nature and cost-efficiency [1–4]. Up to now, researchers have already developed a large number of copper alloys of various systems, such as Cu-Ag, Cu-Cr, Cu-W, Cu-Ni-Si, Cu-Mg, Cu-Ti and Cu-Fe [2,5–21]. Meanwhile, with the rapid advancement of technology, there are increasing demands on small-sized copper alloys used in high-density miniaturized electrical contacts and integrated circuit leads [3,4]. For these special fields, it is required that copper alloys must possess ultra-high strength while maintaining excellent electrical conductivity. For commonly used high-strength electrical contact points, sliding contacts and sliding wires, the required properties typically include the electrical conductivity of over 20 % IACS, the tensile strength of 500–1000 MPa, and the hardness of at least 3 GPa [22]. For example, beryllium copper alloys, which are commonly used for high-strength probes and spring contacts, exhibit a hardness of 3.5–4 GPa, electrical conductivity of 20–22 % IACS, and a tensile strength of 1000–1400 MPa.

* Corresponding author.
** Corresponding author.
*** Corresponding author.
E-mail addresses: jqwang@nimte.ac.cn (J.Q. Wang), huojuntao@nimte.ac.cn (J.T. Huo), gaomeng@nimte.ac.cn (M. Gao).
[1] These authors contributed equally to this work.

https://doi.org/10.1016/j.intermet.2025.108762
Received 16 December 2024; Received in revised form 17 March 2025; Accepted 21 March 2025

However, copper alloys generally have low strength and are prone to softening and deformation, which limits their applicability in these fields. To overcome the bottleneck of the low strength, researchers proposed various strengthening strategies, including grain boundary strengthening, solid solution strengthening, strain strengthening and precipitation strengthening [1–6,11–21]. Unfortunately, in copper alloys, strength and electrical conductivity are not compatible and even opposed. This is because traditional strengthening mechanisms usually increase the yield strength, which leads to electron scattering effect and a loss in conductivity [10–14,23,24]. Therefore, it is crucial to develop new strategies to achieve ultrahigh strength and electrical conductivity in copper alloys to meet the high requirements of high-tech fields, especially the chip industry being closely related to the electrical contacts and circuit leads.

For various metals and alloys, the size deduction usually leads to the increase of the strength and the elongation considering the size effect induced the grain refinement [2,25–28]. What is more, the grain refinement has been verified to be beneficial for the improvement of the electrical conductivity of alloys [29–31]. Meanwhile, for the industrial applications in the field of electrical contacts and circuit leads, small-sized fiber-like metal materials are the first-choice materials to be given top priority. Thus, it is of great importance for developing the alloy fiber with the high strength and conductivity. For the traditional copper alloy fibers, it is usually fabricated by cold drawing technology [32,33]. With increasing tensile strain, cold drawing elongates the grains along the tensile direction and introduces dislocation substructures, significantly enhancing the strength of copper. Nevertheless, it has a detrimental effect to the electrical conductivity since the cold drawing induces a great deal of the lattice distortion, dislocations and the residual stress [23,34,35]. In contrast, recent researches have demonstrated that rapid solidification (melt extraction) shows great potential for the fabrication of fiber alloy materials [36–38]. This processing enables fabrication of alloys with metastable structures and predefined grain size due to the ultrafast cooling rate during solidification. Meanwhile, without the serious deformation, the electron scattering can be enormously reduced during rapid solidification. From this perspective, this fast-cooled melt extraction technology may provide a preferable framework to fabricate the fiber-like copper alloy with the good electrical conductivity.

Except for the typical copper alloys of Cu-Cr-Zr, Cu-Ni-Si, Cu-Ag, Cu-Ti and Cu-Mg, Cu-Pd alloy system has received increasing attention due to its excellent electrical conductivity and mechanical properties [5–9]. From a historical perspective, Pd-Cu alloys were initially used in the field of electrical conductors. However, due to the high cost of palladium and its relatively low strength, alloying became essential. The addition of copper to palladium aimed to enhance mechanical properties through solid solution strengthening while minimizing the loss of electrical conductivity. Since 2010, elements such as Au, Ni, Mg, and Ag have been added to Pd-Cu alloys to enhance their mechanical properties while maintaining good electrical conductivity [39–42]. Recently, alloys with a composition of 44–55 % Cu, 35–45 % Pd, and 6–12 % Ag (atomic percent) are highly favored in the field of electrical contacts [43]. Additionally, researchers have explored the addition of insoluble metals such as ruthenium and rhodium. Platinum group metals are primarily

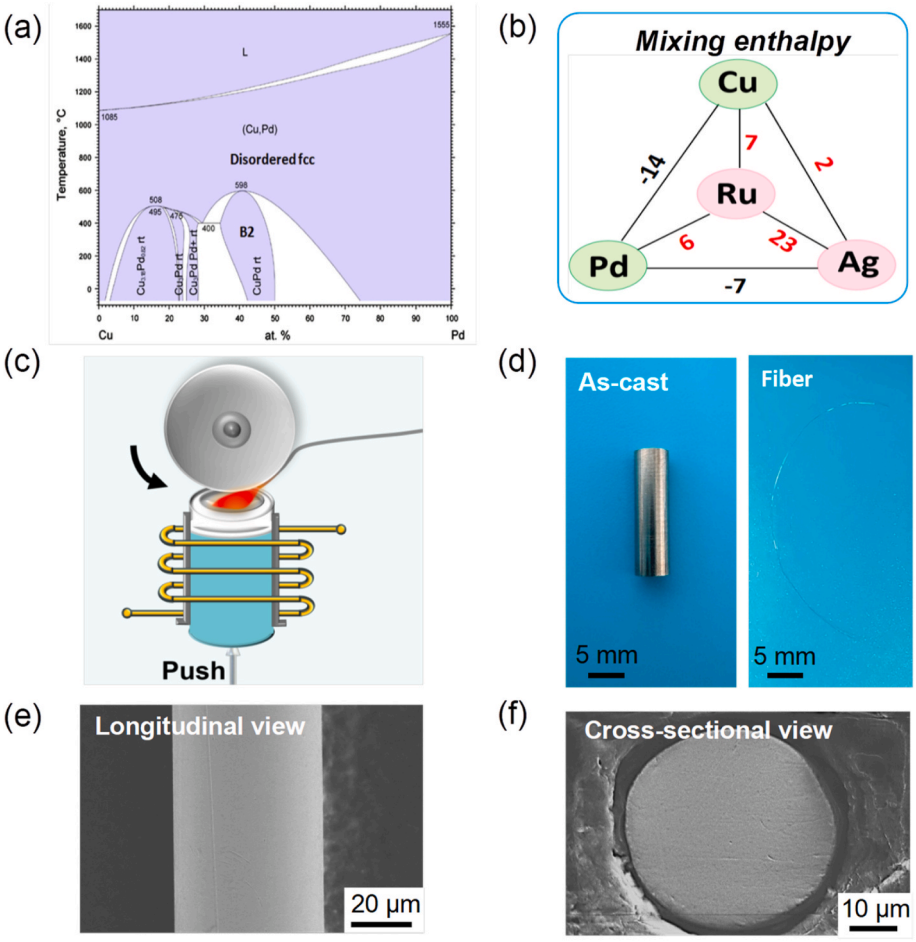

Fig. 1. (a) Phase diagram for the Cu-Pd alloy system. (b) Mixing enthalpy diagram for the elements of Cu, Pd, Ag and Ru. (c) Scheme of alloy-melt extraction process. (d) Optical picture of the $Cu_{44}Pd_{45}Ag_{9.4}Ru_{1.6}$ cast alloy sample (Left) and the alloy microfiber (Right). SEM images of the $Cu_{44}Pd_{45}Ag_{9.4}Ru_{1.6}$ alloy microfiber: (e) Longitudinal view; (f) Cross-sectional view.

chosen due to their melting points and densities being similar to those of palladium, copper, and silver, which simplifies the metallurgical melting process. Moreover, ruthenium and rhodium are less prone to oxidation, further enhancing the material's stability. Currently, Cu-Pd-Ag-Ru quaternary alloys in strip and wire forms are considered highly promising electrical contact materials [44]. However, the fiber-forming process is relatively complex, and the high cost of Ru and Pd, as noble metals, limits large-scale applications.

As seen from the Cu-Pd phase diagram shown in Fig. 1(a), Cu-Pd alloys (36–47 at. % Pd) undergo a structural phase transition below 600 °C, transforming from a disordered FCC structure (A1-type) to an ordered BCC structure (B2-type) [45]. Previous researches reported that the resistivity of the Cu-Pd alloy decreases by nearly tenfold during the phase transformation from A1-type phase to B2-type phase [46,47]. What is more, due to the differing plastic deformation mechanisms of the FCC and BCC phases, the phase transformation from A1-type phase to B2-type phase also contributes to an increase in strength [48]. Therefore, the combination of the enhanced strength and good electrical conductivity may be achieved by introducing a B2 ordered micro-structure into the Cu-Pd copper alloys.

In this work, aimed at the microscale electrical contacts and circuit leads in the field of integrated circuit, we developed one new Cu-Pd-Ag-Ru alloys with combined strength and electrical conductivity by simply melt-extraction and appropriate post-heat treatment. Cu-Pd alloys are widely used in electronic and electrical contact materials due to their excellent electrical conductivity and corrosion resistance. However, their strength and hardness are generally low. Cu-Pd alloys with 36–47 at. % Pd undergo a phase transition below 600 °C, forming an ordered Cu-Pd B2 structure. This crystalline structure significantly enhances the strength of the alloy while maintaining good electrical conductivity. Moreover, minor-alloying is an effective strategy for enhancing the strength of alloys. The doping of Ag and Ru was to introduce the nanoscale strengthening precipitation considering that the positive mixing enthalpy between Ag, Ru and Cu, Pd, further enhancing the alloy's strength [49,50], (as shown in Fig. 1(b)). Thus, based on the above considerations, this study designed the $Cu_{44}Pd_{45}Ag_{9.4}Ru_{1.6}$ (at. %) alloy composition. It was found that the developed $Cu_{44}Pd_{45}Ag_{9.4}Ru_{1.6}$ fiber alloy displays excellent comprehensive properties of strength and electrical conductivity. Compared to the traditional cast alloy, the melt-extracted fiber alloy with order B2 phase has the finer grains and nanoscale precipitations. Finally, the physical mechanism for the enhancement of the strength and electrical conductivity was discussed. The research findings of this work can offer some enlightenment for designing the novel copper alloys for the industrial production and various high-tech applications.

2. Experimental methods

The alloy ingot with the nominal composition of $Cu_{44}Pd_{45}Ag_{9.4}Ru_{1.6}$ (at. %) were fabricated by arc melting pure metals of Cu, Pd, Ag with a purity of 99.99 % and Ru with a purity of 99.95 % in a Ti-gettered high-purity argon atmosphere. To ensure the chemical homogeneity, the ingot was re-melted at least five times and the mass loss of the ingot is less than 0.3 %. Then, the ingot was cut into several small pieces. One of these pieces was firstly melted and was suctioned into the water-cooled copper mold. The diameter of the fabricated rod sample is about 5 mm. Finally, the shredded rod-shaped samples were placed into a glass tube of the melt extraction instrument and the melt-extracted fiber sample can be prepared. The isothermal heat treatment was conducted on the obtained as-cast fiber alloys at 400 °C for 5 h under vacuum.

The information of the microstructure of the prepared $Cu_{44}Pd_{45}Ag_{9.4}Ru_{1.6}$ rod and fiber samples were analyzed thoroughly using various advanced technologies, including X-Ray Diffraction (XRD, Bruker D8), scanning electron microscope (SEM, Zeiss Sigma 300), electron backscattered diffraction (EBSD, Verios G4 UC)), transmission kikuchi diffraction (TKD, 8230) and transmission electron microscope (TEM, Talos F200x). Before the TKD test, the samples were carefully treated by firstly mechanical polishing and then ion beam milling. The formed phases of the prepared $Cu_{44}Pd_{45}Ag_{9.4}Ru_{1.6}$ rod and fiber samples were analyzed using X-ray diffraction (XRD, Bruker D8). The surface morphology of the $Cu_{44}Pd_{45}Ag_{9.4}Ru_{1.6}$ fiber sample was observed using scanning electron microscopy (SEM, Zeiss Sigma 300). The atomic structure for the prepared $Cu_{44}Pd_{45}Ag_{9.4}Ru_{1.6}$ rod and fiber samples were measured by transmission electron microscope (TEM, Talos F200x). The TEM samples were prepared using a focused ion beam (FIB, Helios-G4-CX).

The hardness tests were performed at room temperature using a nanoindenter equipped with a Berkovich diamond indenter tip (Bruker, Hysitron TI980). The tip radius is about 100 nm. The strength was determined by uniaxial tensile tests using a universal testing machine (Zwick/Roell Z1.0) with a constant strain rate of 0.001 s^{-1}. The electrical resistance of the prepared samples was measured by DC resistance meter (CXT 2515) at room temperature. Thus, the corresponding electrical conductivity of these specimens can be calculated using the following equation:

$$EC = \frac{L}{R \bullet S \bullet 58 \bullet 10^6} \bullet 100\% \quad (1)$$

where EC is the relative electrical conductivity, expressed in relation to the International Annealed Cu Standard (% IACS), referred to as the electrical conductivity in the following section; L is the length of the specimen; R is the electrical resistance of the specimen; S is the radial cross-sectional area of the measured specimen. In order to make the data real and reliable, R usually needs to be measured more than three times to confirm the average value. And the electrical conductivity is the average of the three measured values, expressed by % IACS. For ensuring the reproducibility, all of the tests for the strength and the conductivity were repeated at least three times under the same experimental conditions.

3. Results and discussion

3.1. Characterization of surface morphology and phase structure for various $Cu_{44}Pd_{45}Ag_{9.4}Ru_{1.6}$ alloys

To fabricate the fiber-like alloy for the electrical contacts and circuit leads, the melt extraction method was applied and the scheme of the experimental instrument was displayed in Fig. 1(c). For comparison, the 5 mm rod-like sample with the same chemical composition was also prepared by the suction-casting method [51,52]. The optical photos of the prepared fiber and rod samples were exhibited in Fig. 1(d). From Fig. 1(d), it seems that the cast $Cu_{44}Pd_{45}Ag_{9.4}Ru_{1.6}$ fiber displays a smoother and more shining surface compared to that of cast alloy sample. To further check the surface morphology of the cast $Cu_{44}Pd_{45}Ag_{9.4}Ru_{1.6}$ fiber sample, the SEM was used to observe from the longitudinal and cross-section views, respectively. Clearly, there is no obvious surface defects or cracks for the cast $Cu_{44}Pd_{45}Ag_{9.4}Ru_{1.6}$ fiber sample based on the result in Fig. 1(e). What is more, from Fig. 1(f), the diameter of the prepared alloy fiber is about 50 μm. For the melt extraction method, the diameter of the fabricated fiber samples can be precisely controlled by setting the applied rotation speed. Generally, the faster the rotation speed, the smaller the resulting fiber diameter. Thus, the melt extraction technology provides a good and flexible tool to prepare the smooth and size-controllable fiber-like alloys.

To confirm the phase structure of the prepared $Cu_{44}Pd_{45}Ag_{9.4}Ru_{1.6}$ cast alloy and cast fiber samples, the corresponding XRD patterns were obtained and shown in Fig. 2. One can see that the main crystalline phase for the cast alloy and cast fiber is FCC phase. Based on the designing object in Fig. 1(a), the promising crystalline phase is the ordered B2 phase with potential high electrical conductivity and high strength. Previous researches reported that the FCC phase for the cast

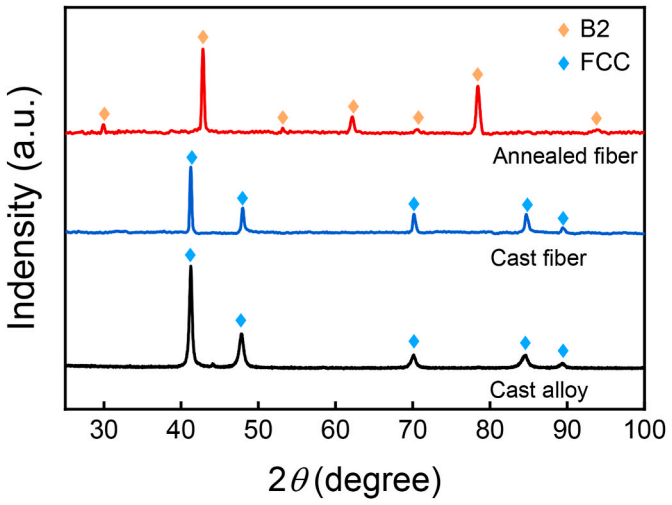

Fig. 2. XRD patterns of the cast alloy, cast $Cu_{44}Pd_{45}Ag_{9.4}Ru_{1.6}$ alloy fiber and annealed $Cu_{44}Pd_{45}Ag_{9.4}Ru_{1.6}$ alloy fiber.

Cu-Pd alloys by electrodeposition and mechanical alloying can be transformed into the B2 phase under 400 °C for 5 h [53–56]. Herein, to obtain the $Cu_{44}Pd_{45}Ag_{9.4}Ru_{1.6}$ fiber alloy with the B2 phase, the same annealing treatment was conducted on the cast fiber sample. And the corresponding XRD pattern was also included in Fig. 2. After annealing treatment, the $Cu_{44}Pd_{45}Ag_{9.4}Ru_{1.6}$ fiber sample displays the complete B2-phase structure. The above results obviously confirm that the combination of the fast-cooled melt extraction and the proper annealing treatment promotes the formation of the B2-ordered microstructure in Cu-Pd alloys. It should be noted that the XRD signal of the formation of nanoscale precipitated phases originated from the minor additions of Ag and Ru does not appear due to the low concentration and the small sizes. Int the below, more detailed experiments will be conducted.

3.2. Mechanical and electrical performance characterization

For the electrical contacts and circuit leads, the combination of the excellent mechanical property and electrical conductivity are crucial. Higher hardness and high strength contribute to the wear resistance and long service life of electrical contact copper alloys. As shown in Fig. 3(a), the hardness of the annealed $Cu_{44}Pd_{45}Ag_{9.4}Ru_{1.6}$ fiber sample was measured using the Continuous Stiffness Measurement (CSM) method based on nanoindentation [57]. $Cu_{44}Pd_{45}Ag_{9.4}Ru_{1.6}$ cast alloy was also used as a reference sample. The nanoindentation continuous load-displacement curves for the annealed fiber and cast alloy samples were plotted in the insertion of Fig. 3(a). Obviously, compared to the cast alloy, the annealed fiber displays an obvious hardening behavior. The corresponding hardness is also consistent with the above hardening phenomenon. The hardness for the annealed fiber sample is 6.22 GPa, which is larger 56 % than that of the cast alloy (3.99 GPa).

To determine the strength of the annealed fiber, tensile tests were conducted on both the annealed fiber and the cast alloy. The corresponding tensile stress-strain curves were presented in Fig. 3(b). For the micro-scale fiber sample, the experimental setup for the tensile test was illustrated in the insertion of Fig. 3(b) [58]. In order to prevent the fiber sample from slipping during tensile deformation, the fiber sample were fixed inside a paper frame and glued firmly. Then, the fiber sample and the paper frame were clamped with a holder, and the two sides of the paper frame were cut off for the tensile test. From Fig. 3(b), one can see that the yielding strength for the $Cu_{44}Pd_{45}Ag_{9.4}Ru_{1.6}$ cast alloy is only 490 MPa. In contrast, the strength for the annealed fiber is about 1350 MPa, resulting in a remarkable enhancement of over 175 % compared to the cast alloy.

For the electrical conductivity, it was measured by the standard four-point probe measurement method and the measurement scheme was shown in the insertion of Fig. 3(c). For each sample, the tests were repeated for at least three times and the detailed values of the electrical conductivity were plotted in Fig. 3(c). One can see that the average electrical conductivity of the annealed $Cu_{44}Pd_{45}Ag_{9.4}Ru_{1.6}$ fiber is about 28.45 % IACS and there is only 16.64 % IACS for the cast alloy. The annealed alloy fiber displays an improvement of over 70 %. This result indicates that the electrical conductivity for the annealed fiber is much higher than that of the cast alloy and it is consistent with our design objective.

To further compare the overall performance of various copper alloys, the plot of the electrical conductivity and the yielding strength for

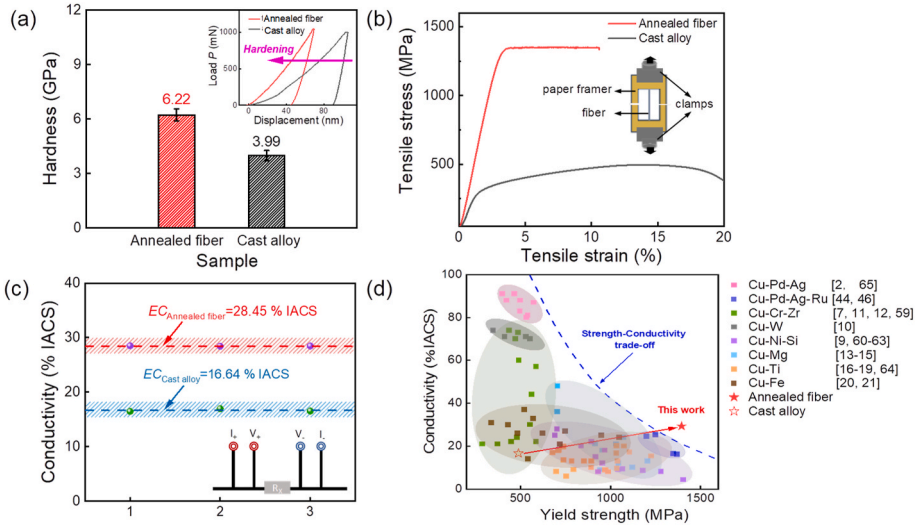

Fig. 3. Characterization of mechanical and conductive properties for the annealed $Cu_{44}Pd_{45}Ag_{9.4}Ru_{1.6}$ alloy fiber and cast alloy. (a) Hardness comparison using the continuous-stiffness-measurement (CSM) based on the nanoindentation. The inserted graph gives the nanoindentation displacement-load curves for two samples. (b) Tensile stress-strain curves for the annealed $Cu_{44}Pd_{45}Ag_{9.4}Ru_{1.6}$ alloy fiber and cast alloy. For microscale fiber sample, the measurement method for the uniaxial tensile test was inserted in Fig. 3(b). (c) Conductivity comparison for the annealed $Cu_{44}Pd_{45}Ag_{9.4}Ru_{1.6}$ alloy fiber and cast alloy. The conductivity measurements were based on the four-terminal method and the scheme was inserted in Fig. 3(c). (d) Plot of yield strength vs. conductivity for various copper alloys [2,7,9–21,44,46,59–65].

various copper alloys was obtained and shown in Fig. 3(d) [2,7,9–21,44,46,59–65]. The detailed values of the strength and conductivity for various copper alloys were included in Table 1. For clarity, the guideline for the trade-off of the strength and conductivity was given by one blue dashed curve in Fig. 3(d) [2,7,9–21,44,46,59–65]. It is clear that the $Cu_{44}Pd_{45}Ag_{9.4}Ru_{1.6}$ cast alloy displays the smaller strength and the conductivity compared to other copper alloys. In contrast, after annealing treatment, the yielding strength for the B2-ordered fiber sample displays 175 % increase and the conductivity displays a 70 % increase. The synchronous improvement of the strength and the conductivity successfully makes the annealed $Cu_{44}Pd_{45}Ag_{9.4}Ru_{1.6}$ fiber overcome the strength-conductivity trade-off for the copper alloys.

3.3. Microstructural characterization of the annealed $Cu_{44}Pd_{45}Ag_{9.}Ru_{1.6}$ alloy fiber

3.3.1. Grain size distribution comparison for the cast alloy and the annealed alloy fiber

From the results in Fig. 2, the phase structures for the cast alloy and the annealed alloy fiber were significantly different. For copper alloys, except for the phase structure, the grain size for different phases is vital for the mechanical and electrical properties. Thus, it is essential to investigate the grain size distribution for the cast alloy and the annealed alloy fiber. Herein, the EBSD tests were used to characterize the spatial distribution of various crystalline phases and the detailed results were exhibited in Fig. 4(a)–(e). Firstly, for the $Cu_{44}Pd_{45}Ag_{9.4}Ru_{1.6}$ cast alloy, there appear various FCC grains with different sizes and there is no grain orientation. To quantitatively obtain the size distribution, the detailed grain size distribution column plot was shown in Fig. 4(b). One can see that the average grain size of the cast alloy is about 15.1 μm. In contrast, as shown in Fig. 4(c) and (d), the grain morphologies along the cross-sectional and longitudinal views exhibit different patterns and the size seems much smaller than that of the cast alloy. Moreover, for the annealed alloy fiber sample, there is also no grain orientation along the cross-sectional view. However, the grains display the obvious orientation along the longitudinal view. The quantitative grain size distributions along the cross-sectional and longitudinal views were displayed in Fig. 4(e). The average grain sizes of the annealed alloy fiber along the cross-sectional and longitudinal views are 80 nm and 275 nm, respectively.

It is noteworthy that the grain size of the annealed $Cu_{44}Pd_{45}Ag_{9.4}Ru_{1.6}$ alloy fiber remains very small compared to that of cast alloy. Considering that the fiber sample is fabricated by the fast-cooled melt extraction method, this fine-grain micro-structure should be originated from this special preparation procedure. Previous researches indicated that the cooling rate for the melt extraction can reach 10^6 K/s [36–38]. Such a high cooling rate significantly enhances the nucleation of the crystals and suppresses the growth of grains, resulting in the formation of ultra-fine grains for the alloy fiber sample. For the elongated grains in Fig. 8(d), it is due to the high rotational speed of the copper wheel during the melt extraction. During this process, considering that the fiber sample is super large aspect ratio, the heat within the melt dissipates more quickly along their length. As a result, the longitudinal temperature gradient is larger, increasing the driving force for crystal growth along the fiber length direction. Additionally, the rapid rotation of the copper wheel exerts a longitudinal force on the alloy fiber, promoting the atomic movement and rearrangement along the direction of the stress, thus facilitating crystal growth in the longitudinal direction [66,67].

Table 1
List of conductivity and yield strength for various Copper alloys.

Cu alloys	Conductivity (% IACS)	Yield strength (MPa)	References
Cu-Ag	80–91	422–541	[83]
Cu-Cr-Zr	21–74	289–587	[7,11,12,22]
Cu-W	70–74	348–554	[10]
Cu-Ni-Si	4–28	692–1405	[9,23,54–56]
Cu-Mg	9–48	707–1207	[13–15]
Cu-Ti	6–20	679–1226	[16–19,57]
Cu-Fe	14–37	337–1049	[20,21]
Cu-Pd-Ag-Ru (cast alloy)	16.45–16.83	485–495	This work
Cu-Pd-Ag-Ru (fiber)	28.41–28.49	1345–1355	This work

3.3.2. Characterization and analyses of the grain structures for the annealed alloy fiber

To investigate the microscopic structure of the annealed alloy fiber, the atomic structure and the chemical composition for the grains need to be confirmed. One local region within the annealed fiber sample was selected and the SEM image was shown in Fig. 5(a). The corresponding EDS maps for different elements were exhibited in Fig. 5(b). Obviously, the solvent elements in the matrix were primarily composed of uniformly distributed Cu and Pd and there is no obvious segregation behavior for these two elements. In contrast, there appear the segregation for the elements of Ag and Ru. Based on the mixing enthalpy diagram in Fig. 1(b), the mixing enthalpy between Ru, Ag and Cu, Pd are positive. The positive mixing enthalpy means it is difficult to form the compound between Ru, Ag and Cu, Pd. What is more, L.A. Lumper et al. found that the addition of Ag and Ru to Cu-Pd alloys does not affect the lattice constant of the Cu-Pd B2 phase [68]. Thus, the addition of the elements of Ru and Ag will lead to the segregation of the added Ru and Ag. The above discussions are in line with the results in Fig. 5(b).

To further quantify the B2 phases and the nanoscale precipitated phases including Ru and Ag, the Transmission Kikuchi diffraction (TKD) was applied. The TKD patterns and the corresponding phase fractions of different grain phases (B2 phase, Ru precipitate phase and Ag precipitate phase) within the annealed $Cu_{44}Pd_{45}Ag_{9.4}Ru_{1.6}$ alloy fiber along the cross-sectional and longitudinal view were separately displayed in Fig. 6 (a)-6(d). Clearly, the B2 phase is the dominant crystalline phase in the annealed $Cu_{44}Pd_{45}Ag_{9.4}Ru_{1.6}$ alloy fiber, comprising over 90 % of the total phase fraction. The Ru precipitates are primarily located at grain boundaries, while the Ag precipitates are distributed both at grain boundaries and within the B2 phase. On the other hand, along the cross-sectional view, the Ag precipitated phase is much more than the Ru precipitated phases. In contrast, along the longitudinal view, the fraction of the Ru precipitated phase is very close to that of the Ag precipitated phase.

For different phases in the annealed $Cu_{44}Pd_{45}Ag_{9.4}Ru_{1.6}$ alloy fiber, the high-resolution transmission electron microscopy (HRTEM) was used to uncover the atomic structure of these phases. The detailed results about the B2 phase and the precipitated phases were shown in Figs. 7 and 8, respectively. Firstly, from Fig. 7(a)-7(g), the HRTEM images and the corresponding selected area electron diffraction (SAED) patterns along different crystal zone axes were obtained. The detailed crystal lattice parameter was also marked. It is clear that the primary crystalline phase of the annealed $Cu_{44}Pd_{45}Ag_{9.4}Ru_{1.6}$ alloy fiber is in agreement with the electron diffraction spots of the Cu-Pd B2 phase, which is consistent with XRD analysis in Fig. 2.

In view of the nanoscale of the Ru and Ag precipitated phases, two magnified EDS images including one Ru precipitate and one Ag precipitate were provided in Fig. 8(a) and (d). Fig. 8(b) and (e) separately display the corresponding TEM images. One can see that small amounts of Ru and Ag precipitates were identified within the B2 phase matrix. Fig. 8(c) and (f) show HRTEM images of the Ru and Ag precipitates, along with their corresponding fast Fourier transform (FFT) images. From the FFT images, the crystal structures of both the Ru and Ag precipitates are hexagonal crystal structure, which is significantly different from the B2 phase of the alloy matrix. Moreover, the average sizes of the Ru and Ag precipitates are about 70 nm and 40 nm, respectively. Compared to the B2 phases, the Ru and Ag precipitates are much smaller

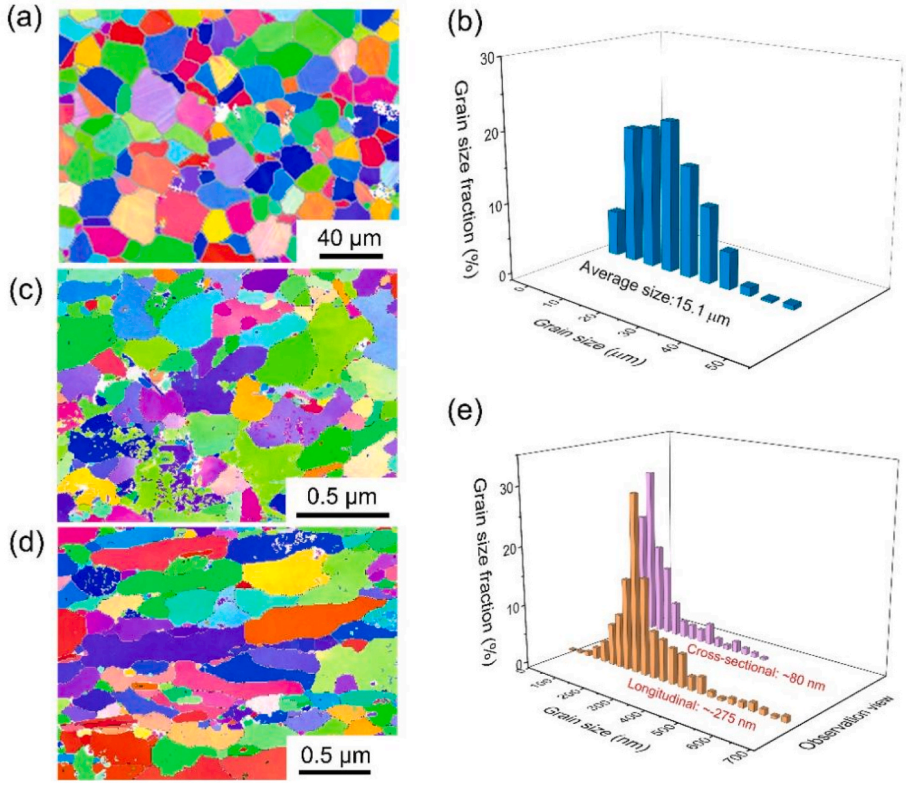

Fig. 4. (a) Grain morphology of the $Cu_{44}Pd_{45}Ag_{9.4}Ru_{1.6}$ cast alloy. (b) Grain size distribution of the $Cu_{44}Pd_{45}Ag_{9.4}Ru_{1.6}$ cast alloy. Grain morphologies of the annealed $Cu_{44}Pd_{45}Ag_{9.4}Ru_{1.6}$ alloy fiber along cross-sectional (c) and longitudinal views (d). (e) Grain size distribution comparison for the annealed $Cu_{44}Pd_{45}Ag_{9.4}Ru_{1.6}$ alloy fiber along cross-sectional and longitudinal views.

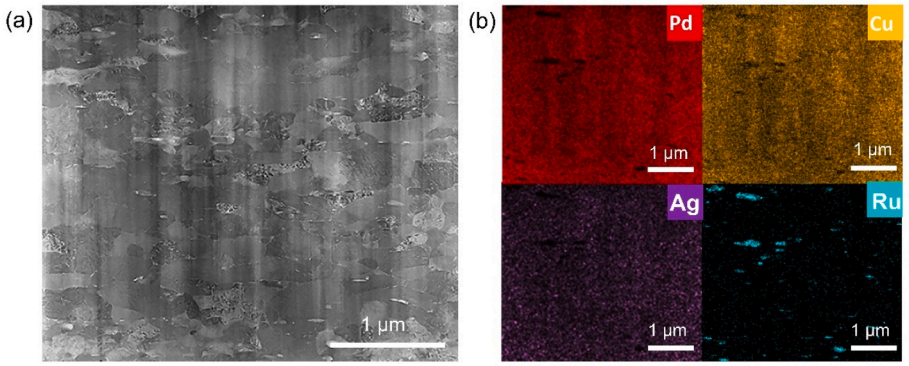

Fig. 5. (a) SEM image of the annealed $Cu_{44}Pd_{45}Ag_{9.4}Ru_{1.6}$ alloy fiber. (b) Elemental maps of annealed $Cu_{44}Pd_{45}Ag_{9.4}Ru_{1.6}$ alloy fiber.

than that of the primary B2 phases, which can be considered as the precipitation strengthening. To more illustrate the influences of the melt extract and the isothermal annealing treatment on the $Cu_{44}Pd_{45}Ag_{9.4}Ru_{1.6}$ alloy, one scheme was proposed in Fig. 9.

3.4. *Physical mechanism of excellent strength-conductivity synergy for the annealed $Cu_{44}Pd_{45}Ag_{9.4}Ru_{1.6}$ alloy fiber*

The developed $Cu_{44}Pd_{45}Ag_{9.4}Ru_{1.6}$ alloy fiber by combining the melt extraction and the appropriate post-heat treatment displays the excellent strength-conductivity synergy. Especially, the strength for the annealed alloy fiber is increased by 2.75 times compared to that of the bulk cast alloy. And the conductivity also increases by 70 %. As shown in Fig. 3(d), our proposed experimental strategy successfully surmounts the strength-conductivity trade-off for the copper alloys. According to the experimental results in Figs. 4–8, the strengthening mechanism for the annealed $Cu_{44}Pd_{45}Ag_{9.4}Ru_{1.6}$ alloy fiber can be explained in the below.

(i) Strengthening from annealing treatment induced the phase transition from FCC phase to B2 phase. For different phases, the deformation behaviors are usually controlled by the dislocation slip. Although both FCC phase and B2 phase have 12 slip systems, the slip directions in the FCC phase are more numerous. It means the FCC crystals have better ductility, which is in line with the results in Fig. 3(b). In contrast, due to the less slip directions, the B2 phase can more effectively resist the dislocation slip when subjected to stress, leading to its higher strength [68]. What is more, in the B2 phase, the increased atomic packing density means that dislocations encounter greater energy barriers during

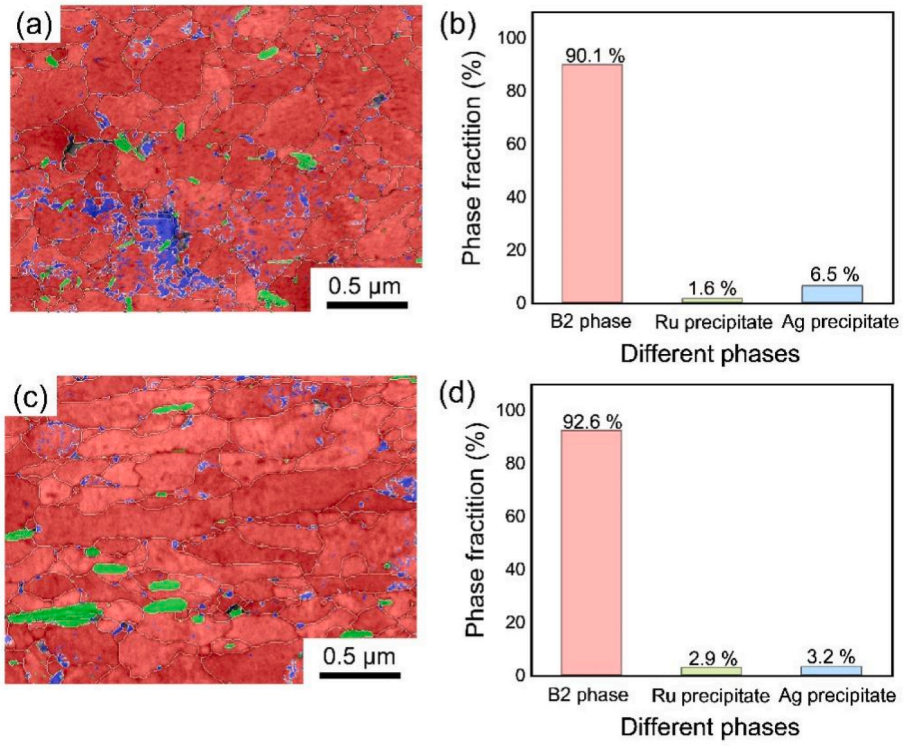

Fig. 6. TKD patterns and the corresponding phase fractions of different grain phases (B2 phase, Ru precipitate phase and Ag precipitate phase) within the annealed $Cu_{44}Pd_{45}Ag_{9.4}Ru_{1.6}$ alloy fiber along the cross-sectional (a, b) and longitudinal (c, d) view.

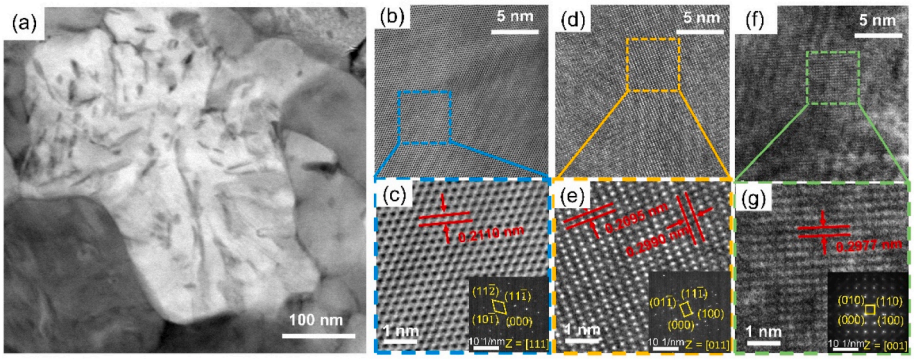

Fig. 7. (a) Bright-field TEM image of one B2 phase within the annealed $Cu_{44}Pd_{45}Ag_{9.4}Ru_{1.6}$ alloy fiber. High-resolution TEM images of annealed $Cu_{44}Pd_{45}Ag_{9.4}Ru_{1.6}$ alloy fiber and corresponding selected-area electron diffraction patterns along different crystal zone axes: (b–c) along the [111] zone axis; (d–e) along the [011] zone axis; (f–g) along the [001] zone axis.

slip [69,70]. This also makes the alloy be less susceptible to dislocation slip under external loads, thereby enhancing its strength.

(ii) Strengthening caused by grain refinement. Compared to the cast $Cu_{44}Pd_{45}Ag_{9.4}Ru_{1.6}$ alloy, the size of the grains of the annealed $Cu_{44}Pd_{45}Ag_{9.4}Ru_{1.6}$ alloy fiber has been reduced by two to three orders of magnitude. The grain refinement results in an increased number of grain boundaries that can more effectively hinder the dislocation slip movement. Additionally, the blocked dislocations near grain boundaries may accumulate and interact with each other, further enhancing the strength of the alloy fiber [71,72].

(iii) Strengthening caused by nano-precipitates. For the annealed $Cu_{44}Pd_{45}Ag_{9.4}Ru_{1.6}$ alloy fiber, there appear a great deal of nanoscale Ru and Ag precipitates among the B2 grains. Firstly, compared to the B2 phase (the average grain sizes along the cross-sectional and longitudinal views are 80 nm and 275 nm), the average sizes of the Ru and Ag precipitates are about 70 nm and 40 nm. The smaller nanoscale precipitates effectively impede the movement of dislocations, thereby increasing the strength and hardness of alloys. Moreover, both the Ag precipitates and the Ru precipitates are hexagonal close-packed (HCP) (Fig. 8(c) and (f)). For HCP structure, there is the limited slip systems [73]. The limited sip system makes the dislocation movement become more difficult and thereby enhances the alloy's strength. In contrast, FCC structures have more slip systems, allowing dislocations to move more easily, which can reduce strength [74].

Subsequently, we will quantitatively analyze the contributions of different strengthening mechanisms in the strength of $Cu_{44}Pd_{45}Ag_{9.4}Ru_{1.6}$ alloy fiber. Firstly, we consider the strengthening effect of grain boundary strengthening on the overall strength. The influence of grain size on the yield strength of the alloy is determined by the Hall-

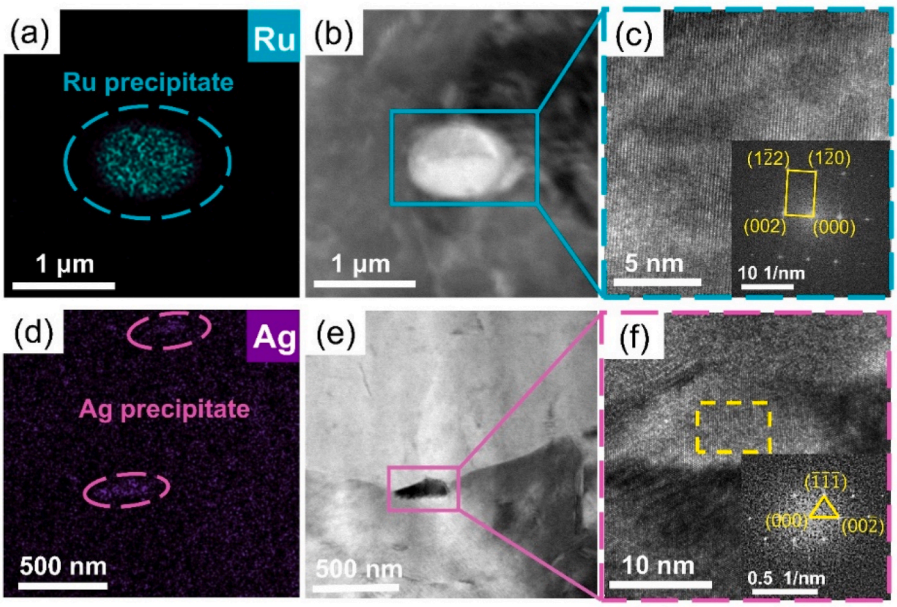

Fig. 8. Characterization of Ru precipitate within the annealed $Cu_{44}Pd_{45}Ag_{9.4}Ru_{1.6}$ alloy fiber: (a) Spatial distribution of Ru element; (b) Corresponding bright-field image; (c) HRTEM image and the corresponding FFT pattern. Characterization of Ag precipitate within the annealed $Cu_{44}Pd_{45}Ag_{9.4}Ru_{1.6}$ alloy fiber: (d) Spatial distribution of Ru element; (e) Corresponding bright-field image; (f) HRTEM image and the corresponding FFT pattern.

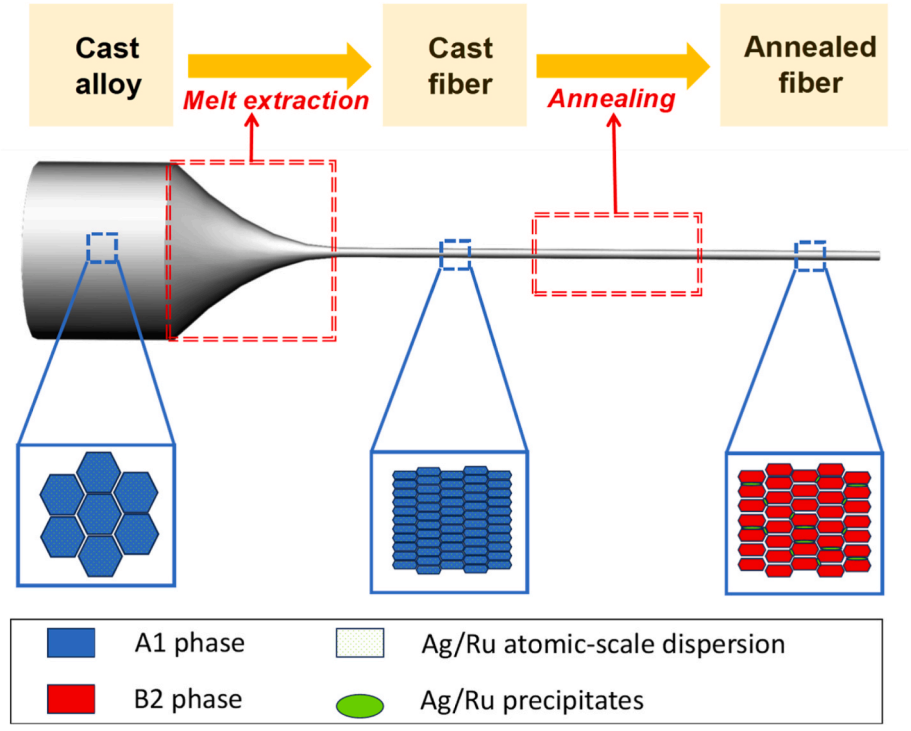

Fig. 9. Scheme of the designing strategy for the Cu-Pd-Ag-Ru alloy microfiber with strength-conductivity synergy and the evolution of the corresponding microscopic structures.

Petch relationship [75], as expressed below:

$$\Delta\sigma_{H-P} = \sigma_0 + kd^{-1/2} \quad (2)$$

where σ_0 represents the lattice frictional resistance when moving a single dislocation, σ_0 can be calculated using the formula $\sigma_0 \approx \frac{Gb}{2\pi} e^{-\frac{2\pi w}{b}}$, k is the Hall-Petch constant, which can be calculated using the formula $k \approx \alpha G\sqrt{b}$, where G is the shear modulus of Cu-Pd, b is its Burgers vector, w is the dislocation width, and α is a constant with a value of 0.4 [75]. The calculation results show that the values of σ_0 and k are 494 MPa and 310 MPa $\mu m^{1/2}$, respectively. And d is the average size of the fiber grains. From this calculation, the grain boundary strengthening yield strength of the $Cu_{44}Pd_{45}Ag_{9.4}Ru_{1.6}$ alloy fiber is determined to be 1185 MPa.

Secondly, as shown in Fig. 6, nanoscale Ag precipitates and Ru precipitate phases are present in the $Cu_{44}Pd_{45}Ag_{9.4}Ru_{1.6}$ alloy fiber,

contributing to precipitation strengthening. The work of Xie [76] indicates that Ag precipitates in the form of band-like particles with a width of approximately 10 nm, which serve as precipitate strengthening phase. These precipitates contribute to the enhancement of fiber strength. The strength of the Ag precipitation and Ru precipitation can be calculated using Eq. (3) [2]:

$$\Delta\sigma_{os} = \frac{0.81Gb}{2\pi(1-\nu)^{1/2}} \frac{\ln(2r/b)}{\lambda - 2r} \tag{3}$$

$$\lambda = r\left[\left(\frac{2\pi}{3f}\right)^{\frac{1}{2}} - 1.63\right] \tag{4}$$

where ν is Poisson's ratio, which is 0.367 in the Cu-Pd matrix [77]; r is the average radius and f is volume fraction of the precipitated phase. From Fig. 6, it can be determined that the volume fractions (f) of the Ag and Ru precipitates are 3.2 % and 2.9 % respectively, while the average grain sizes (r) are 25.6 nm and 83.9 nm. Based on Eq. (3), the contributions of the Ag and Ru precipitates to the strength of the fiber are calculated to be 88 MPa and 30 MPa, respectively.

Lastly, Fig. 2 presents the X-ray diffraction (XRD) pattern of the $Cu_{44}Pd_{45}Ag_{9.4}Ru_{1.6}$ alloy fibers. Due to the low concentrations of Ag and Ru, no distinct diffraction peaks are observed in the XRD pattern aside from those corresponding to the Cu-Pd B2 phase. The intensity of the diffraction peaks for the Cu-Pd B2 phase is affected by the presence of the Ag and Ru precipitates. The dislocation density (ρ) of the fibers was calculated using the Williamson-Hall method [78] based on the XRD pattern.

$$\beta\cos\theta = \frac{K\lambda}{D} + (4\sin\theta)\varepsilon \tag{5}$$

$$\rho = 2\sqrt{3}\Big/(D/b) \tag{6}$$

where β is the half-width peak of the diffraction peak; θ is the Bragg angle; λ is the wavelength of Cu-Kα radiation ($\lambda = 0.15405$ nm); D is the grain size; ε is the microstrain; ρ is the dislocation density; b is the Burgers vector of the Cu-Pd matrix, the value is 0.3 nm. The microstrain (ε) and the grain size (D) values are obtained through linear fitting of Eq. (5). And the value of dislocation density (ρ) can be obtained through Eq. (6). The increase in strength resulting from dislocation strengthening can be calculated using the following equation [78]:

$$\Delta\sigma_d = M\alpha Gb\rho^{1/2} \tag{7}$$

where M is the taylor factor, which is 2.75 for body-centered cubic; α is a constant, for Cu-Pd phase the value is 0.4 [79]; G is the shear modulus of the Cu-Pd B2 matrix, which has a value of 54.6 GPa [77]. Based on Eq. (7), the contribution of dislocation strengthening to the strength is calculated to be 28 MPa.

The strength of the $Cu_{44}Pd_{45}Ag_{9.4}Ru_{1.6}$ alloy fibers can be expressed using Eq. (9):

$$\sigma = \Delta\sigma_{H-P} + \Delta\sigma_{OS} + \Delta\sigma_d \tag{9}$$

The final calculation results reveal the strengthening contributions of various mechanisms in the $Cu_{44}Pd_{45}Ag_{9.4}Ru_{1.6}$ alloy fiber. The strength of the $Cu_{44}Pd_{45}Ag_{9.4}Ru_{1.6}$ alloy fiber produced via melt extraction method is primarily attributed to grain refinement, while the contributions from dislocation strengthening and precipitation strengthening are relatively minor. The calculated ultimate tensile yield strength is 1331 MPa, which is close to the experimental value of 1350 MPa, the error is within 5 %.

For traditional copper alloys, there exists a great deal of various microstructural defects: grain boundaries, dislocations, and vacancies. These defects can interfere with the free movement of electrons, leading to a decrease in electrical conductivity [80–82]. From this perspective, the $Cu_{44}Pd_{45}Ag_{9.4}Ru_{1.6}$ alloy fiber with finer grains and the nanoscale precipitates should have the lower electrical conductivity. Nevertheless, the annealed alloy fiber displays a 70 % enhancement of the conductivity compared to the cast alloy. Considering that there appears the phase transition from the FCC phase to the B2 phase, it means that this phase transition is sufficient to make up for the decline in electrical conductivity caused by defects, and even greatly increase the electrical conductivity. Previous researches reported that the atomic ordering can atomic ordering significantly enhances the electrical conductivity of Cu-Pd alloys [46,47]. Thus, the high electrical conductivity of the annealed $Cu_{44}Pd_{45}Ag_{9.4}Ru_{1.6}$ alloy fiber can primarily be attributed to the highly ordered atomic arrangement within the ordered B2 phase. This ordered structure minimizes lattice defects, enhancing electron transport efficiency. In addition, in the ordered B2 phase, the stronger metallic bonding results in reduced interatomic distances. The strong metallic bonds may lead to smaller band gaps, facilitating easier excitation of electrons during conduction and further enhancing conductivity.

It should be noted that, due to the residual stress and the larger temperature gradient along the longitudinal view during melt extraction, the grains in the annealed $Cu_{44}Pd_{45}Ag_{9.4}Ru_{1.6}$ alloy fiber tended to grow more easily along the longitudinal direction. As a result, the grains in the annealed $Cu_{44}Pd_{45}Ag_{9.4}Ru_{1.6}$ alloy fiber are predominantly columnar rather than equiaxed. This greatly reduces the number of grain boundaries encountered by electrons during longitudinal electrical transport, thereby advancing the electrical conductivity of the annealed alloy fiber. Meanwhile, the high hardness usually means the high wear resistance and long service life, which is also good for the electrical contacts and circuit leads. Therefore, the $Cu_{44}Pd_{45}Ag_{9.4}Ru_{1.6}$ alloy fiber produced via melt extraction and annealing treatment exhibit exceptional strength-conductivity performance, which provides one kind of good candidate materials for the microscale electrical contacts and circuit leads in the field of integrated circuit. On the other hand, there exist some problems for the developed $Cu_{44}Pd_{45}Ag_{9.4}Ru_{1.6}$ alloy fiber. For example, the addition of the noble metals (Pd, Ru) largely increases the production cost of the alloys. And the high melting point of Ru usually leads to composition segregation, while brittle intermetallic compounds at the fiber-matrix interface increase processing complexity. For these problems, it will need more studies to investigate and solve them.

4. Conclusions

In summary, by combing the melt extraction and proper isothermal annealing treatment, we designed one $Cu_{44}Pd_{45}Ag_{9.4}Ru_{1.6}$ alloy fiber material with the excellent strength-conductivity synergy. The main conclusions are.

(1) Compared to the cast alloy, the annealed alloy fiber displays the yielding strength of 1350 MPa, the hardness of 6.22 GPa and the electrical conductivity of 28.45 %IACS. This comprehensive performance of the strength and the conductivity successfully overcome the strength-conductivity trade-off relationship for the copper alloys.
(2) Main strengthening contributions for the annealed alloy fiber are grain refinement, phase transition strengthening, and nano-precipitation strengthening. In comparison with the cast $Cu_{44}Pd_{45}Ag_{9.4}Ru_{1.6}$ alloy, the size of the grains of the annealed alloy fiber has been reduced by two to three orders of magnitude. What is more, the average grain size of B2 phase along the cross-sectional and longitudinal views are 80 nm and 275 nm. In contrast, the average sizes of the Ru and Ag precipitates are about 70 nm and 40 nm. All of the above strengthening contributions have been quantitatively estimated.
(3) Although the refined grain and the nano-precipitates induce a certain degree of sacrifice in electrical conductivity, the ordered B2 phase significantly enhances their electrical conductivity. Additionally, the elongated grains along the longitudinal

direction reduce the impact of grain boundaries on conductivity. The current work offers a novel experimental strategy for overcoming the strength-conductivity trade-off in metallic materials.

CRediT authorship contribution statement

Y.Y. Sun: Writing – original draft, Resources, Methodology, Investigation, Formal analysis. **Y.H. Gao:** Validation, Methodology, Formal analysis. **Y.B. Wang:** Writing – original draft, Resources, Methodology, Formal analysis. **Y. Huang:** Methodology, Formal analysis. **M.C. Jian:** Validation. **F.C. Wang:** Methodology. **Y. Li:** Formal analysis. **L. Fu:** Methodology, Formal analysis. **X. Jin:** Resources. **H.B.C. Yin:** Resources. **J. Xu:** Validation, Methodology. **S.D. Feng:** Validation. **J.Q. Wang:** Writing – review & editing, Project administration, Funding acquisition. **J.T. Huo:** Writing – review & editing, Supervision, Funding acquisition, Conceptualization. **M. Gao:** Writing – review & editing, Supervision, Project administration, Funding acquisition, Conceptualization.

Declaration of competing interest

The authors declare that they have no known competing financial interests or personal relationships that could have appeared to influence the work reported in this paper.

Acknowledgments

This research was supported by the National Natural Science Foundation of China (52201194, 52471187, 52222105, 92163108, 52231006, 52301224, 52301223), 3315 Innovation Youth Talent in Ningbo City (2021A123G), Youth Innovation Promotion Association CAS (2019296), Zhejiang Provincial Natural Science Foundation Regional Innovation and Development Joint Foundation with Quzhou City (LZY23E010002), the Natural Science Foundation of Ningbo City (2023J342, 2023J346, 2024Z075). This research was also supported by Zhejiang Provincial Natural Science Foundation of China (No. LR22E010004, LQ24E010004).

Data availability

Data will be made available on request.

References

[1] H. Yang, Z. Ma, C. Lei, L. Meng, Y. Fang, J. Liu, H. Wang, High strength and high conductivity Cu alloys: a review, Sci. China Technol. Sci. 63 (12) (2020) 2505–2517.
[2] L.W. Kong, X.L. Zhu, Z.B. Xing, Y.Q. Chang, H. Huang, Y. Shu, Z.X. Qi, B. Wen, P. Li, Preparation and mechanisms of Cu–Ag alloy fibers with high strength and high conductivity, Mater. Sci. Eng., A 895 (2024) 146219.
[3] Q. Mao, Y. Liu, Y. Zhao, A review on copper alloys with high strength and high electrical conductivity, J. Alloys Compd. 990 (2024) 174456.
[4] K. Yang, Y. Wang, M. Guo, H. Wang, Y. Mo, X. Dong, H. Lou, Recent development of advanced precipitation-strengthened Cu alloys with high strength and conductivity: a review, Prog. Mater. Sci. 138 (2023) 101141.
[5] L. Sun, N. Tao, K. Lu, A high strength and high electrical conductivity bulk CuCrZr alloy with nanotwins, Scr. Mater. 99 (2015) 73–76.
[6] R. Mishnevn, I. Shakhova, A. Belyakov, R. Kaibyshev, Deformation microstructures, strengthening mechanisms, and electrical conductivity in a Cu-Cr-Zr alloy, Mater. Sci. Eng., A 629 (2015) 29–40.
[7] M. Gholami, J. Vesely, I. Altenberger, H.A. Kuhn, M. Janecek, Effects of microstructure on mechanical properties of CuNiSi alloys, J. Alloys Compd. (2017) 201–212.
[8] S. Gorsse, B. Ouvrard, M. Gouné, A. Poulon-Quintin, Microstructural design of new high conductivity – high strength Cu-based alloy, J. Alloys Compd. 633 (2015) 42–47.
[9] G.A. Xin, M. Zhou, K. Jing, H. Hu, Z.A. Li, Y. Zhang, Q. Bai, C. Tian, B. Tian, X. Li, A.A. Volinsky, J. Zou, Heat treatment effects on microstructure and properties of Cu–Ti–Fe alloys, Mater. Sci. Eng., A 892 (2024) 146048.
[10] D. Li, Q. Wang, B. Jiang, X. Li, W. Zhou, C. Dong, H. Wang, Q. Chen, Minor-alloyed Cu-Ni-Si alloys with high hardness and electric conductivity designed by a cluster formula approach, Prog. Nat. Sci. 27 (4) (2017) 467–473.
[11] L.C. Zhuo, J.L. Zhang, Q.Q. Zhang, H.L. Wang, Z. Zhao, Q.Y. Chen, S.L. Liang, J. T. Xu, A.Y. Xi, Achieving both high conductivity and reliable high strength for W–Cu composite alloys using spherical initial powders, Vacuum 181 (2020) 109720.
[12] A.H. Huang, Y.F. Wang, M.S. Wang, L.Y. Song, Y.T. Zhu, Optimizing the strength, ductility and electrical conductivity of a Cu-Cr-Zr alloy by rotary swaging and aging treatment, Mater. Sci. Eng., A 746 (2019) 211–216.
[13] J. Huang, Z. Xiao, J. Dai, Z. Li, H. Jiang, W. Wang, X. Zhang, Microstructure and properties of a novel Cu-Ni-Co-Si-Mg alloy with super-high strength and conductivity, Mater. Sci. Eng., A 744 (2019) 754–763.
[14] L. Si, L. Zhou, X. Zhu, S.H. Li, S. Leinuo, Q.Y. Dong, Microstructure and property of Cu-2.7Ti-0.15Mg-0.1Ce-0.1Zr alloy treated with a combined aging process, Mater. Sci. Eng. A (650) (2016) 345–353.
[15] Y. Li, Z. Xiao, Z. Li, Z. Zhou, Z. Yang, Q. Lei, Microstructure and properties of a novel Cu-Mg-Ca alloy with high strength and high electrical conductivity, J. Alloys Compd. 723 (2017) 1162–1170.
[16] K. Yang, M. Guo, H. Wang, M. Wang, Y. Mo, Y. Wang, F. Liu, D. Liang, H. Lou, Synergistically improved strength and electrical conductivity of Cu-3.3 wt%Ti alloy via coupling control of dislocation and multi-scale precipitates, Mater. Sci. Eng., A 915 (2024) 147259.
[17] B. Rouxel, C. Cayron, J. Bornand, P. Sanders, R.E. Logé, Micro-addition of Fe in highly alloyed Cu-Ti alloys to improve both formability and strength, Mater. Des. 213 (2022) 110340.
[18] Y. Tu, X. Liu, W. Wang, W. Zhang, Q. Feng, Deformation-aging behavior and property evolution of Cu–Ti alloys prepared by accumulative roll bonding-deformation diffusion process, Mater. Sci. Eng., A 855 (2022) 143915.
[19] Y. Fu, G. Xie, F. Zhao, J. Wan, X. Meng, X. Liu, R. Wang, X. Liu, Precipitation behaviors and property variations of Cu-3.0 wt% Ti fabricated by a novel short-processing non-vacuum heating-cooling combined mold continuous casting, J. Alloys Compd. 921 (2022) 166059.
[20] F. Yang, L. Dong, L. Zhou, N. Zhang, X. Zhou, X. Zhang, F. Fang, Excellent strength and electrical conductivity achieved by optimizing the dual-phase structure in Cu–Fe wires, Mater. Sci. Eng., A 849 (2022) 143484.
[21] Y. Wu, W. Zhang, Y. Li, F. Yang, H. Liu, J. Zou, J. Jiang, F. Fang, A. Ma, An overview of microstructure regulation treatment of Cu-Fe alloys to improve strength, conductivity, and electromagnetic shielding, J. Alloys Compd. 1002 (2024) 175425.
[22] B.D. Beake, A.J. Harris, T.W. Liskiewicz, J. Wagner, S.J. McMaster, S.R. Goodes, A. Neville, L. Zhang, Friction and electrical contact resistance in reciprocating nano-scale wear testing of metallic materials, Wear 474 (2021) 203866.
[23] P.V. Andrews, M.B. West, C.R. Robeson, The effect of grain boundaries on the electrical resistivity of polycrystalline copper and aluminium, Philos. Mag. 19 (161) (1969) 887–898.
[24] Feldman Baruch, Park Seongjun, Haverty Michael, Shankar Sadasivan, T. Scott, Simulation of grain boundary effects on electronic transport in metals, and detailed causes of scattering, Phy. status. solidi (b). 247 (7) (2010) 1791–1796.
[25] D. Li, C. Li, T. Feng, Y. Zhang, G. Sha, J.J. Lewandowski, P.K. Liaw, Y. Zhang, High-entropy Al0.3CoCrFeNi alloy fibers with high tensile strength and ductility at ambient and cryogenic temperatures, Acta Mater. 123 (2017) 285–294.
[26] Y. Sakai, H.J. Schneidei-Muntau, Ultra-high strength, high conductivity Cu-Ag alloy wires, Acta Mater. 45 (1997) 1017–1023.
[27] K. Wei, R. Hu, D. Yin, L. Xiao, S. Pang, Y. Cao, H. Zhou, Y. Zhao, Y. Zhu, Grain size effect on tensile properties and slip systems of pure magnesium, Acta Mater. 206 (2021) 116604.
[28] J.M. Wheeler, C. Kirchlechner, J.-S. Micha, J. Michler, D. Kiener, The effect of size on the strength of FCC metals at elevated temperatures: annealed copper, Philos. Mag. 96 (32–34) (2016) 3379–3395.
[29] M.Y. Murashkin, I. Sabirov, X. Sauvage, R.Z. Valiev, Nanostructured Al and Cu alloys with superior strength and electrical conductivity, J. Mater. Sci. 51 (1) (2015) 33–49.
[30] L. Dong, F. Yang, T. Yu, N. Zhang, X. Zhou, Z. Xie, F. Fang, Contribution of grain boundary to strength and electrical conductivity of annealed copper wires, J. Mater. Res. Technol. 26 (2023) 1459–1468.
[31] S.F. Abbas, S.-J. Seo, K.-T. Park, B.-S. Kim, T.-S. Kim, Effect of grain size on the electrical conductivity of copper–iron alloys, J. Alloys Compd. 720 (2017) 8–16.
[32] K. Hanazaki, N. Shigeiri, N. Tsuji, Change in microstructures and mechanical properties during deep wire drawing of copper, Mater. Sci. Eng., A 527 (21–22) (2010) 5699–5707.
[33] H. Park, S.-H. Kim, W.-J. Lee, J.-W. Ha, S.-J. Kim, H.-J. Lee, Effect of wire-drawing process conditions on secondary recrystallization behavior during annealing in high-purity copper wires, Met. Mater. Int. 27 (7) (2020) 2220–2229.
[34] F. Yang, L. Dong, L. Cai, L. Wang, Z. Xie, F. Fang, Effect of cold drawing strain on the microstructure, mechanical properties and electrical conductivity of low-oxygen copper wires, Mater. Sci. Eng., A 818 (2021) 141348.
[35] J.P. Hou, R. Li, Q. Wang, H.Y. Yu, Z.J. Zhang, Q.Y. Chen, H. Ma, X.M. Wu, X.W. Li, Z.F. Zhang, Three principles for preparing Al wire with high strength and high electrical conductivity, J. Mater. Sci. Technol. 35 (5) (2019) 742–751.
[36] G. Geng, D. Wang, W. Zhang, L. Liu, A.M. Laptev, Fabrication of Cu–Ni–Si alloy by melt spinning and its mechanical and electrical properties, Mater. Sci. Eng., A 776 (2020) 138979.
[37] V.I. Tkatch, A.I. Limanovskii, S.N. Denisenko, S.G. Rassolov, The effect of the melt-spinning processing parameters on the rate of cooling, Mater. Sci. Eng., A 323 (2002) 91–96.
[38] J.Q. Feng, Y.H. Liu, J.H. Sui, A.N. He, W.X. Xia, W.H. Wang, J.Q. Wang, J.T. Huo, Giant refrigerant capacity in Gd-based amorphous/nanocrsytalline composite fibers, Mater. Today. Phy. 21 (2021) 100528.

[39] K.E. Coulter, J.D. Way, S.K. Gade, S. Chaudhari, D.S. Sholl, L. Semidey-Flecha, Predicting, fabricating, and permeability testing of free-standing ternary Palladium−Copper−Gold membranes for hydrogen separation, J. Phys. Chem. C 114 (40) (2010) 17173–17180.
[40] C. Ling, L. Semidey-Flecha, D.S. Sholl, First-principles screening of PdCuAg ternary alloys as H2 purification membranes, J. Membr. Sci. 371 (1) (2011) 189–196.
[41] A.M. Tarditi, F. Braun, L.M. Cornaglia, Novel PdAgCu ternary alloy: hydrogen permeation and surface properties, Appl. Surf. Sci. 257 (15) (2011) 6626–6635.
[42] T.A. Peters, T. Kaleta, M. Stange, R. Bredesen, Development of thin binary and ternary Pd-based alloy membranes for use in hydrogen production, J. Membr. Sci. 383 (1) (2011) 124–134.
[43] A.S. Klein, E.E.I. Smith, S. Viswanathan, High-Strength Conductive Alloy Fibers for Electrical Contacts, 2017. US20170218481.
[44] W. Huang, H. Yu, L. Wang, X. Wu, C. Ouyang, Y. Zhang, J. He, State of the art and prospects in sliver- and copper-matrix composite electrical contact materials, Mater. Today Commun. 37 (2023) 107256.
[45] L. M, Alloy Phase Diagrams, ASM, 2016.
[46] A.Y. Volkov, Improvements to the microstructure and physical properties of Pd-Cu-Ag alloys, Platin. Met. Rev. 48 (1) (2004) 3–12.
[47] O.V. Antonova, O.S. Novikova, B.D. Antonov, A.Y. Volkov, Evolution of the microstructure and mechanical properties of the Cu-47Pd (at %) alloy during atomic ordering after severe plastic deformation, Phys. Met. Metallogr. (2015) 401–412.
[48] A.Y. Volkov, O.S. Novikova, A.E. Kostina, B.D. Antonov, Effect of alloying with palladium on the electrical and mechanical properties of copper, Phys. Met. Metallogr. 117 (9) (2016) 945–954.
[49] J.P. Chu, C.H. Lin, V.S. John, Cu films containing insoluble Ru and RuNX on barrierless Si for excellent property improvements, Appl. Phys. Lett. 91 (13) (2007) 132109.
[50] S. Dasari, Studying the effect of ruthenium on high temperature mechanical properties of nickel based superalloys and determining the universal behavior of ruthenium at atomic scale with respect to alloying elements, stress and temperature, Res. Ideas. Outcomes. 2 (2016) e10714.
[51] A.R. Balpande, S. Agrawal, X. Li, S. Suwas, S. Guo, P. Ghosal, S.S. Nene, Excellent specific strength-ductility synergy in novel complex concentrated alloy after suction casting, Mater. Des. 242 (2024) 112988.
[52] Z. Szklarz, H. Krawiec, Ł. Rogal, The effect of vacuum suction casting on the microstructure and corrosion behavior of aluminium alloy 2017, Mater. Sci. Eng., B 240 (2019) 23–32.
[53] L. Tian, A. Russell, T. Riedemann, S. Mueller, I. Anderson, A deformation-processed Al-matrix/Ca-nanofilamentary composite with low density, high strength, and high conductivity, Mater. Sci. Eng., A 690 (2017) 348–354.
[54] J. Tosques, M.H. Martin, L. Roué, D. Guay, Hydrogen solubility in PdCuAg ternary alloy films prepared by electrodeposition, Int. J. Hydrogen Energy 39 (28) (2014) 15810–15818.
[55] J. Galipaud, M.H. Martin, L. Roué, D. Guay, Pulsed laser deposition of PdCuAu alloy membranes for hydrogen absorption study, J. Phys. Chem. C 119 (47) (2015) 26451–26458.
[56] J. Galipaud, M.H. Martin, L. Roué, D. Guay, Measurement of hydrogen solubility in PdxCu100–xThin films prepared by pulsed laser deposition: an electrochemical in situ X-ray diffraction analysis, J. Phys. Chem. C 117 (6) (2013) 2688–2698.
[57] X. Li, B. Bhushan, A review of nanoindentation continuous stiffness measurement technique and its applications, Mater. Char. 48 (2002) 11–36.
[58] J. Yi, H.Y. Bai, D.Q. Zhao, M.X. Pan, W.H. Wang, Piezoresistance effect of metallic glassy fibers, Appl. Phys. Lett. 98 (24) (2011).
[59] R. Li, H. Kang, Z. Chen, G. Fan, C. Zou, W. Wang, S. Zhang, Y. Lu, J. Jie, Z. Cao, A promising structure for fabricating high strength and high electrical conductivity copper alloys, Sci. Rep. 6 (1) (2016) 20799.
[60] S. Zhang, R. Li, H. Kang, Z. Chen, W. Wang, C. Zou, T. Li, T. Wang, A high strength and high electrical conductivity Cu-Cr-Zr alloy fabricated by cryorolling and intermediate aging treatment, Mater. Sci. Eng., A 680 (2017) 108–114.
[61] L. Shen, Z. Li, Z. Zhang, Q. Dong, Z. Xiao, Q. Lei, W. Qiu, Effects of silicon and thermo-mechanical process on microstructure and properties of Cu–10Ni–3Al–0.8Si alloy, Mater. Des. 62 (2014) 265–270.
[62] H.G. Chen, H.S. Wang, J.W. Gu, C.E. Hsu, C.Y. Wu, Effects of heat treatment processes on the microstructures and properties of powder metallurgy produced Cu-Ni-Si-Cr alloy, Mater. Sci. Eng., A 619 (2014) 221–227.
[63] L. Shen, Z. Li, Q. Dong, Z. Xiao, Q. Lei, Dry wear behavior of ultra-high strength Cu-10Ni-3Al-0.8Si alloy, Tribol. Int. 92 (2015) 544–552.
[64] L. Liu, W. Yang, M. Fang, H. Li, J. Mo, H. Liu, F. Li, N. Song, Effects of B2 ordered structure on the mechanical properties of TiZrHfCoNiCu high-entropy alloy, Mater. Today Commun. 39 (2024) 2769–2782.
[65] Y. Zhang, H. Guo, J. Cao, X. Wu, H. Jia, A. Chang, Research progress of palladium-plated copper bonding wire in microelectronic packaging, Micromachines 14 (8) (2023).
[66] W.F. Smith, Principles of Materials Science and Engineering, 1986.
[67] S.H. Avner, Introduction to Physical Metallurgy, 1964.
[68] L.A. Lumper, J. Fecher, A. Stark, K. Maier, Verena, investigation of phase transformations and ordering mechanisms in a Pd–Cu–Ag–Ru alloy, Adv. Eng. Mater. (2024) 1–10.
[69] X. Ye, W. Xu, Z. Li, D. Xu, W. Zhang, B. Li, D. Fang, Microstructures and mechanical properties of FeNiCrMnAl high-entropy alloys, J. Mater. Eng. Perform. 31 (10) (2022) 7820–7829.
[70] D.D. Zhang, J.Y. Zhang, J. Kuang, G. Liu, J. Sun, The B2 phase-driven microstructural heterogeneities and twinning enable ultrahigh cryogenic strength and large ductility in NiCoCr-based medium-entropy alloy, Acta Mater. 233 (2022) 117981.
[71] X. Zhu, Z. Xiao, J. An, H. Jiang, Y. Jiang, Z. Li, Microstructure and properties of Cu-Ag alloy prepared by continuously directional solidification, J. Alloys Compd. 883 (2021) 160769.
[72] N. Kamikawa, T. Hirochi, T. Furuhara, Strengthening mechanisms in ultrafine-grained and sub-grained high-purity aluminum, Metall. Mater. Trans. 50 (1) (2018) 234–248.
[73] M.H. Yoo, S.R. Agnew, J.R. Morris, K.M. Ho, Non-basal slip systems in HCP metals and alloys: source mechanisms, Mater. Sci. Eng. 319–321 (2001) 87–92.
[74] Y. Pan, Pressure induced structural, hardness, elastic and thermodynamic properties of three MoC, Int. J. Refract. Metals Hard Mater. 115 (2023) 106277.
[75] N. Hansen, Hall–Petch relation and boundary strengthening, Scr. Mater. 51 (8) (2004) 801–806.
[76] M. Xie, W. Huang, H. Chen, L. Gong, W. Xie, H. Wang, B. Yang, Microstructural evolution and strengthening mechanisms in cold-rolled Cu–Ag alloys, J. Alloys Compd. 851 (2021).
[77] M.C. Gao, L. Ouyang, Ö.N. Doğan, First principles screening of B2 stabilizers in CuPd-based hydrogen separation membranes: (1) Substitution for Pd, J. Alloys Compd. 574 (2013) 368–376.
[78] J. Freudenberger, J. Lyubimova, A. Gaganov, H. Witte, A.L. Hickman, H. Jones, M. Nganbe, Non-destructive pulsed field CuAg-solenoids, Mater. Sci. Eng., A 527 (7–8) (2010) 2004–2013.
[79] D.B. Miracle, Overview No. 104 the physical and mechanical properties of NiAl, Acta Metall. Mater. 41 (3) (1993) 649–684.
[80] N.Q. Chinh, J. Gubicza, T.G. Langdon, Characteristics of face-centered cubic metals processed by equal-channel angular pressing, J. Mater. Sci. 42 (5) (2007) 1594–1605.
[81] K. Ma, H. Wen, T. Hu, T.D. Topping, J.M. Schoenung, Mechanical behavior and strengthening mechanisms in ultrafine grain precipitation-strengthened aluminum alloy, Acta Mater. 62 (5) (2014) 141–155.
[82] J.P. Hou, R. Li, Q. Wang, H.Y. Yu, Z.J. Zhang, Q.Y. Chen, H. Ma, X.M. Wu, X.W. Li, Z.F. Zhang, Breaking the trade-off relation of strength and electrical conductivity in pure Al wire by controlling texture and grain boundary, J. Alloys Compd. 769 (2018) 96–109.
[83] T. Ichitsubo, E. Matsubara, T. Yamamoto, H.S. Chen, N. Nishiyama, J. Saida, K. Anazawa, Microstructure of fragile metallic glasses inferred from ultrasound-accelerated crystallization in Pd-based metallic glasses, Phys. Rev. Lett. 95 (2005) 245501.